Biobased Nanocomposites Prepared by In Situ Polymerization of Furfuryl Alcohol with Cellulose Whiskers or Montmorillonite Clay

Lawrence Pranger*,† and Rina Tannenbaum*,†,‡

School of Materials Science and Engineering, Georgia Institute of Technology, Atlanta, Georgia 30332, Department of Chemical Engineering, Technion - Israel Institute of Technology, Haifa 32000, Israel

Received September 4, 2008; Revised Manuscript Received September 23, 2008

ABSTRACT: In this work, we employed an in situ polymerization approach to produce polyfurfuryl alcohol (PFA) nanocomposites without the use of solvents or surfactants. On the one hand, furfuryl alcohol (FA) has a dual function, serving both as an effective dispersant for the cellulose whisker (CW) and montmorillonite clay (MMT) nanoparticles and as the matrix precursor for the in situ polymerization. On the other hand, the CW and MMT nanoparticles also serve multiple functions, by first catalyzing the polymerization of FA, and then acting as an effective matrix modifier, increasing the thermal stability of the consolidated PFA nanocomposite. In the case of CW-PFA nanocomposites, the polymerization is catalyzed by sulfonic acid residues at the CW surface, left over from the whisker preparation. In the case of MMT-PFA nanocomposites, the polymerization is catalyzed by Lewis acid sites inherent to the MMT surface. Thermal analysis showed that both types of polymer nanocomposites (PNCs) were characterized by significantly higher temperature at the onset of degradation and higher residual weight after nonoxidative degradation compared to unmodified PFA. Most importantly, by choosing PFA as the matrix and nanoparticles of CW and MMT, we were able to produce nanocomposites that are not only marked by high thermal resistance, but which were produced entirely from biobased precursor materials.

1. Introduction

A polymer matrix nanocomposite (PNC) is defined as a polymer matrix, in which nanoparticles (i.e., having a length, width or thickness in the range of 1−100 nm) have been evenly dispersed. The nanoparticle phase has a significantly higher surface area compared to most traditional fillers. For example, nanoparticles of cellulose have a surface area in the range of 150−170 m^2/g, while nanoclays may have surface areas as high as 750 m^2/g.[1−4] When dispersed in composite matrix, the high surface area of the nanoparticle phase leads to high interfacial area between matrix and filler, and to the immobilization of the matrix polymer at the nanoparticle surface. As a result, significant enhancements in thermo-mechanical performance are often observed for PNCs compared to conventional composites, for example, increased glass transition temperature, flame retardancy, and onset of degradation.[5] Unfortunately, the high surface area of the nanoparticles poses a significant processing challenge, because the van der Waals attraction between particles and the high viscosity of the matrix polymer makes it difficult to produce stable, uniform dispersions of the nanoparticles throughout the matrix.

To overcome these factors and achieve the desired dispersion of nanoparticles in PNCs, techniques involving suspensions mixing have been used.[1,6] These techniques are suitable for casting films, however, significant amounts of solvent (water or other diluents, depending on the nanoparticle and polymer systems used) must be evaporated during the matrix consolidation process. In contrast to this approach, the in situ intercalative polymerization technique has been successfully used (such as in the case of MMT-containing PNCs) to produce a range of PNCs without the use of dilution or surfactants.[5] The main advantage of this approach is the fact that the "solvent" molecules (i.e., molecules that constitute the low viscosity medium in which the nanoparticles form a stable suspension) act also as the monomer system. Hence, once the dispersion of the nanoparticles in this "solvent" is achieved, the ensuing in situ polymerization traps the nanoparticles in the forming matrix, thus ensuring the homogeneity of the PNC.

Biobased PNCs are of particular interest today, because they have the potential to replace materials traditionally derived from the petrochemical supply chain.[7] Such PNCs could be comprised of biopolymer matrices embedded with nanoparticles whose origins could be found either as naturally occurring minerals or as renewable plant feedstocks. One particular biopolymer, polyfurfuryl alcohol (PFA) is of remarkable interest due to its commercial availability, low viscosity, which lends it to applications involving in situ polymerization, and finally, its compatibility with hydrophilic nanoparticles. Surprisingly, PFA has received little attention to date, compared to other biopolymers. While PFA is hydrophobic, its monomer precursor furfuryl alcohol (FA), is hydrophilic and completely soluble in water, due to the hydroxyl group of the side chain and the oxygen heteroatom of the furan ring. The presence of these functional groups in FA makes this monomer able to stabilize suspensions of hydrophilic nanoparticles such as, for example, the hydroxylated surfaces of CW and MMT. FA is produced from its corresponding aldehyde, furfural, by hydrogenation. Furfural (furfur = bran) is prepared in commercial quantities from pentose-rich agricultural residues, including rice hulls, bagasse, oat hulls, and corn cobs. Furfural can also be derived from wood and wood products, which represent a second natural storehouse for furfural.[8] The resinification of FA was reported on as early as 1873.[9] In the early stages of resinification, FA polymerizes predominantly through "head-to-tail" reactions, in which the hydroxymethylene function of one molecule reacts with the hydrogen at the C5 position of the furan ring of a second molecule, yielding a methylene bridge. "Head-to-head" condensation between hydroxymethylene groups, yielding dimethylene ether bridges, also occurs at this stage. In addition, levulinic acid and lactone byproducts may be produced as a result of hydrolytic ring cleavage of furan rings.[9] Cross-linking occurs in the later stages of resinification. The mechanism responsible for this cross-linking process is still not completely

* To whom correspondence should be addressed. E-mail: rinatan@mse.gatech.edu or rinatan@technion.ac.il (R.T.); lawrence.pranger@mse.gatech.edu (L.P.).
† Georgia Institute of Technology.
‡ Technion - Israel Institute of Technology.

10.1021/ma8020213 CCC: $40.75 © 2008 American Chemical Society
Published on Web 10/28/2008

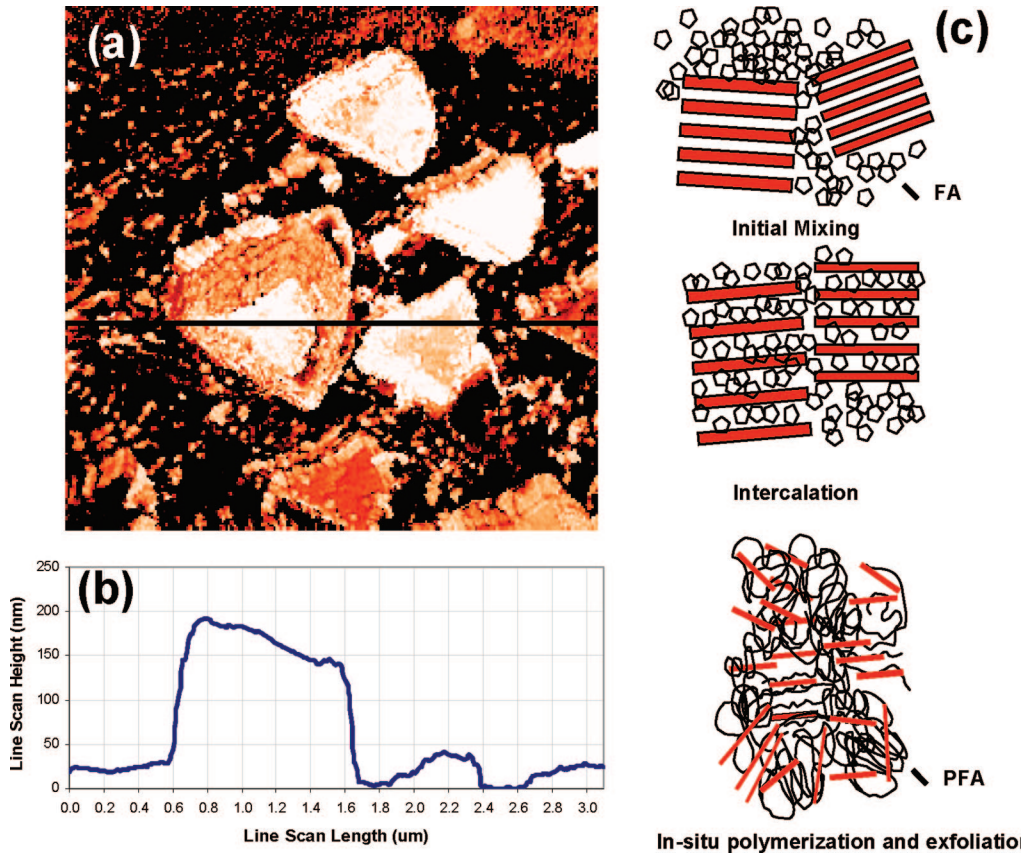

Figure 1. (a) AFM phase contrast image of tactoids of sodium montmorillonite showing its lamellar morphology. (b) Line scan from corresponding z-height image. The position of the line scan is indicated by the bar in the phase contrast image. Note that the image size is 3.1 μm. (c) Schematic representation of the in situ intercalative polymerization.

understood.[10−12] The first step involves the formation of unsaturated sequences along the PFA chain backbone.[10] The second step may involve condensation between reactive hydrogen atoms along these unsaturated sequences and terminal hydroxyl groups of neighboring chains. The role of formaldehyde, which is split off when dimethyl ether bridges decompose to methylene bridges, is not clear. The polymerization of FA is normally catalyzed using a Brönstedt acid, for example, sulfuric, hydrochloric, and *para*-toluene sulfonic acid (PTSA). Overcatalysis with strong mineral acids such as these may lead to an explosive reaction. To avoid this risk, polymerization can also be achieved in the presence of Lewis acids, for example, γ-alumina.

In this work we explore the formation of PFA nanocomposites by the in situ polymerization of FA using either MMT or CW as the particulate phase. We will exploit the chemical functionalities of FA to effectively disperse cellulose whisker (CW) or montmorillonite clay (MMT) nanoparticles, while also using FA as the monomer precursor for the in situ polymerization to form the PFA matrix. Also the CW and MMT nanoparticles serve multiple functions, as they are capable both of catalyzing the polymerization of FA, and acting as effective matrix modifiers, increasing the thermal stability of the consolidated PFA nanocomposites. It is noteworthy that by choosing PFA as the matrix and nanoparticles of CW and MMT, we will be able to produce nanocomposites from precursor materials that can be sourced entirely outside the petrochemical supply chain.

2. Experimental Section

2.1. Materials and Methods. Two types of MMT, sodium montmorillonite (Cloisite Na, Southern Clay) and an organomodified montmorillonite (Cloisite 30B), were used to prepare MMT-PFA nanocomposites, coded NaMMT-PFA and 30BMMT-PFA, respectively. The organic modifier in Cloisite 30B is methyl, tallow, bis-2-hydroxyethyl, quaternary ammonium, where tallow is 65% C18, 30% C16, and 5% C14. Cellulose whiskers were prepared, starting from MCC precursor (Avicel, Aldrich) to streamline the procedure. The main steps in the whiskers synthesis were (i) acid hydrolysis (62% H_2SO_4, 55 °C, 2 h), (ii) refining and purification of the solid residue remaining after the hydrolysis by repeated 20−40 min cycles of ultra centrifuging at 10000 rpm followed by resuspension of the solids in distilled water until turbid supernatant was obtained, (iii) dialysis against distilled water to pH 5−6, and (iv) freeze-drying. To confirm this procedure yields CW with the desired nanoscale morphology, concentrated CW suspensions were viewed through crossed polars and birefringence observed at rest. To estimate the aspect ratio of the whiskers, AFM (see below) was performed on dried films of dilute CW suspensions.

MMT-PFA resins were produced by charging FA (99% pure, Sigma-Aldrich) and 10 phr MMT (parts per hundred resin, actually FA) to a round-bottom flask. To achieve intercalation, the mixture was homogenized by vigorous agitation with a magnetic stir bar and slowly heating to the target reaction temperature of 150 °C. To provide a basis for comparison with PFA modified with CW and MMT, pure PFA resin was prepared by reacting FA with 5 phr (parts per hundred resin) γ-alumina (nanopowder, Aldrich) at 100 °C for 12 h (denoted GAl-PFA). This resin was stable during storage (at room temperature) for several months. The composite curing cycle was confirmed by DSC. After oven-curing of the CW-PFA, MMT-PFA, and GAl-PFA resins at 130 °C for 75 min and then at 210 °C for 105 min, no residual cure exotherm was observed in DSC scans but only a broad decomposition peak with a peak max at around 360 °C.

2.2. Characterization Techniques. All AFM images of MMT and CW were collected in close contact mode using silicon tips, on a Pacific Nanotechnology scanner, varying the scanning frequency between 0.5 − 1 Hz, and z-setpoint as required for each

scan. X-ray diffraction data was collected on a Rigaku Miniflex diffractometer, at a scanning rate of 0.5 degrees s^{-1}, using Cu Kα radiation with a wavelength of $\lambda = 1.54$ Å. FTIR data was collected on a Thermo Nicolet Nexus 870 unit, using ZnSe windows. A minimum of 50 scans were collected at a resolution of 2 cm^{-1}. TGA data was collected on a TA Instruments Q50, at a heating rate of 10 °C/min. Samples were heated up to 800 °C under a flow of 25 $mL \cdot min^{-1}$ nitrogen.

3. Results and Discussion

3.1. In Situ Polymerization of Furfuryl Alcohol Using Montmorillonite Nanoclays. The various stages of the in situ intercalative polymerization of FA using MMT nanoclays are described in Figure 1. MMT is a layered silicate belonging to the 2:1 phyllosilicate (phyllo = leaf) family and consists of stacks of thin platelets. Each individual platelet consists of an octahedral alumina sheet, sandwiched between two tetrahedral silica sheets (hence, the 2:1 ratio). The platelets have a net negative charge due to substitution of some of the Al^{3+} cations with Mg^{2+} ions. This charge is counterbalanced by inorganic cations, for example, Na^{+} confined to interlayer galleries between platelets. This causes platelets to form stacks ("tactoids") held together by electrostatic forces. Figure 1a is an AFM image showing several tactoids of naturally occurring montmorillonite clay, to illustrate its lamellar morphology. Each individual platelet has a thickness of approximately 1 nm.[3] From the line scan, Figure 1b, it can be seen that the aspect ratio for MMT platelets is in the range of 20−100. The in-plane modulus for a single platelet of MMT has been estimated as 400 GPa. However, the bulk modulus of MMT, which includes the contribution of the nonload bearing interlayer gallery, is roughly 270 GPa.[13] The first step in the in situ intercalative polymerization of PFA involves the intercalation of FA in the interlayer galleries of MMT tactoids, as schematically depicted in Figure 1c. Because FA is hydrophilic, while PFA is hydrophobic, the intercalation process was studied both with naturally occurring hydrophilic sodium montmorillonite (NaMMT) and with an organomodified montmorillonite (30BMMT). The next step in the in situ intercalative polymerization involves the polymerization of the intercalated FA inside the interlayer galleries, which forces apart the individual platelets of the MMT tactoids. Preliminary DSC surveys (see Supporting Information) indicated that MMT possesses sufficient catalytic activity (attributed to Lewis acidity) to effect the polymerization of FA to PFA above approximately 140 °C. Therefore, upon heating the system to the target temperature of 150 °C, both NaMMT-FA and 30BMMT-FA mixtures resinified, reaching the gel point within 1−2 h.

Intercalation and exfoliation of MMT leads to an increase in the d_{001} spacing (i.e., the basal spacing) of the MMT tactoids, which can be calculated from the position of the main diffraction peak in XRD and from Braggs law, $2d \sin \theta = \lambda$. The interlayer gallery spacing can then be estimated by subtracting 10 Å (the thickness of a single platelet) from the calculated basal spacing. Figure 2 shows the various stages of exfoliation of MMT as a function of polymerization of PFA. Figure 2a, patterns a−c, shows the diffraction patterns collected for the 30BMMT-PFA resin. Prior to intercalation, 30BMMT powder (pattern a) has a basal spacing of $d_{001} = 17.2$ Å ($2\theta = 5.1°$) and hence an interlayer gallery spacing of approximately 7.2 Å. This spacing is due to the organic modifier being oriented roughly parallel to the platelets. In the initial 30BMMT-FA mixture, the basal spacing increases by approximately 20 Å, evidenced by a dramatic shift in the main diffraction peak from 5.1 to 2.4 Å, showing that 30BMMT is readily dispersed in FA. Interestingly, this basal spacing remains nearly constant as the intercalated FA undergoes resinification. At the gel point of the 30BMMT-PFA resin (pattern b), some 30BMMT tactoids remain intact

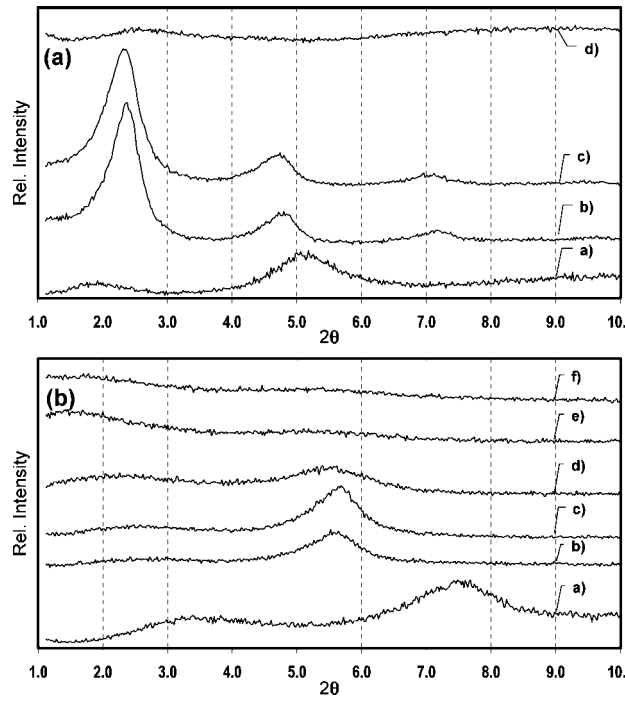

Figure 2. XRD patterns showing intercalation and exfoliation of MMT as a function of polymerization of PFA. The top graph (a) shows (line a) 30BMMT; (line b) intercalated 30BMMT PFA resin; (line c) 30BMMT PFA resin after first stage cure; and (line d) fully cured and exfoliated 30BMMT PNC. The bottom graph (b) shows XRD patterns for (line a) NaMMT; (line b) after initial mixing with FA; (lines c−e) intercalated NaMMT PFA resin at 130 °C, 140 and 150 °C, respectively; and (line f) exfoliated NaMMT PFA resin.

albeit with a slightly increased basal spacing of 18.3 Å ($2\theta = 4.8°$). However, most of the 30BMMT is intercalated with PFA, as evidenced by the intense diffraction peak at 37.1 Å ($2\theta = 2.4°$), which corresponds to an interlayer gallery spacing of 27 Å. 30BMMT-PFA resin produced using a Brönstedt acid as a cocatalyst was also found to be intercalated, with nearly the same basal spacing (37 Å). At this stage, the organic modifier is envisioned as forming a paraffinic monolayer, in which the tallow chain of the organomodifier is extended away from the clay surface, to optimize solvation by the intercalating monomer or polymer.[14] The observed basal spacing is close to that described for 30BMMT intercalated with epoxy precursor (DGEBA), and for octadecyl ammonium-modified MMT intercalated with polyols with molecular weights ranging from 700−3000 g/mol.[15,16] In the latter case, the interlayer gallery expansion was shown to depend on the chain length of the organic modifier, rather than the molecular weight of the intercalating polyol. Strong diffraction peaks were still observed at $2\theta = 2.4°$ and 4.8° in the 30BMMT-PFA nanocomposite after the first stage of curing at 130 °C (pattern c), but not in the final cured 30BMMT-PFA nanocomposite (pattern d), showing that the 30BMMT has been exfoliated throughout the matrix. The exfoliation has presumably been achieved by stiffening of the PFA due to extended cross-linking and molecular weight increase during the second stage of curing. In the case of NaMMT, exfoliation is achieved already upon resinification. Figure 2b shows that prior to intercalation, NaMMT powder (pattern a) has a basal spacing of $d_{001} = 11.7$ Å ($2\theta = 7.5°$) corresponding to an interlayer gallery spacing of approximately 1.7 Å. NaMMT, like 30BMMT, is readily dispersed in FA, and after initial mixing (pattern b), it undergoes an interlayer gallery expansion to approximately 15.5 Å ($2\theta = 5.7°$). At this stage, a monolayer of FA is most likely coordinated to the surface of the NaMMT clay by hydrogen bonding. As the reaction temperature increases to 130−140 °C (patterns c,d),

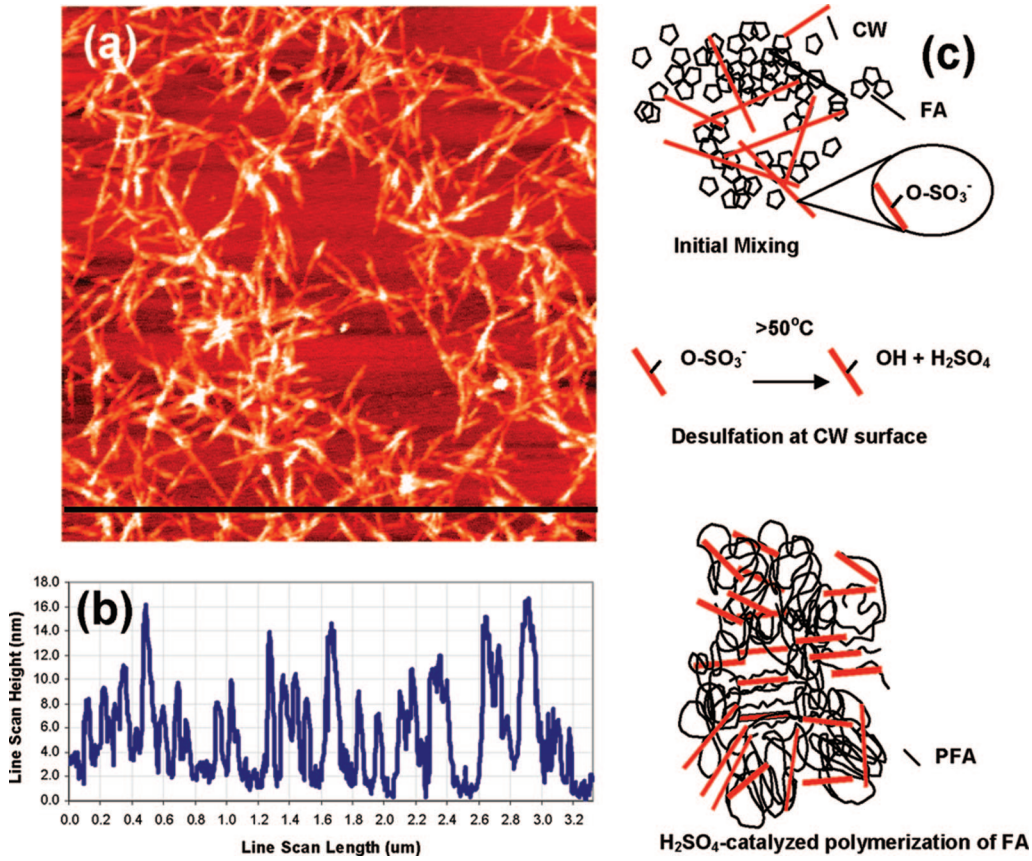

Figure 3. (a) AFM z-height image of cellulose whiskers from acid hydrolysis of microcrystalline cellulose. (b) Line scan, the position of which is indicated by the bar in the z-height image. Note that the image size is 3.3 μm. (c) Schematic representation of the in situ polymerization of CW-PFA nanocomposites.

resinification proceeds more rapidly, the diffraction peak broadens, its intensity decreases, and by the time the temperature reaches 150 °C (pattern e), the peak vanishes, indicating complete exfoliation of NaMMT-PFA resin (pattern f). Together with the XRD results from the cured 30BMMT-PFA nanocomposite, this shows that the in situ intercalative polymerization is especially favorable for the MMT-FA combination. While the MMT initially functions as a catalyst in the polymerization of FA, the polymerization of FA and cross-linking of PFA in turn, promote the exfoliation of MMT.

3.2. In Situ Polymerization of Furfuryl Alcohol Using Cellulose Whiskers. Figure 3 describes the in situ intercalative polymerization of FA using CW nanoparticles. The needle-like morphology of CW produced from acid hydrolysis of microcrystalline cellulose (MCC) is shown in Figure 3a. From the AFM line scan in Figure 3b, it can be seen that the average diameter of these whiskers is 10 nm, and the aspect ratio is in the range of 50−100. The high aspect ratio of CW enables them to form a rigid network of particles above the percolation threshold concentration, which can be achieved with as low as 1 wt %, and this also contributes to the enhanced mechanical properties of CW PNCs.[17,18] Strong intermolecular hydrogen-bonding in CW gives it a very high degree of crystallinity and a high elastic modulus. For crystalline cellulose, estimates for the longitudinal modulus vary in the range of 100−150 GPa, with an average value of 130 GPa, which is comparable to aramid fiber.[1,18−20] CW has a richly hydroxylated surface, and when sulfuric acid is used in the CW synthesis, the CW surface also contains sulfonic acid residues originating from the hydrolysis step.[2,4] The sulfonic acid groups carry a negative charge, and this is critical for providing electrostatic stabilization of the CW dispersion in the FA. However, the de-esterification of these sulfonic acid groups from the CW surface at elevated temperature can be exploited to catalyze the in situ polymerization of FA in close proximity to the CW. By wrapping PFA around the CW, the initial particle dispersion can be preserved in the PFA resin and in the cured nanocomposite. To explore this approach, shown schematically in Figure 3c, 0.75−1.0 phr freeze-dried CW was dispersed in FA by means of a brief ultrasonication treatment (Fisher 500W, 25−50% amplitude, 15 min) followed by heating to 50 °C for 1 h. At this temperature, the CW-FA mixture was stable, and the rate of polymerization was negligible. However, increasing the reaction temperature to the 75−100 °C range immediately triggered the polymerization of FA. Within 2−3 min, the mixture turned from yellow to dark brown due to rapid accumulation of PFA particles. After 4 h at 75 °C, a fluid resin was obtained, however, at 100 °C, the gel point was reached within 2 h. Under identical experimental conditions, neither microcrystalline cellulose (MCC) nor silica gel induced the polymerization of FA, demonstrating that neither the ultrasonication treatment, nor the presence of a high, hydroxyl-rich surface area is sufficient to explain the rapid polymerization of FA in the presence of CW. Rather, it is the sulfonic acid residues at the CW surface that are responsible for triggering the polymerization. At room temperature and up to 50 °C, the sulfonic acid groups at the CW surface are stable. However, increasing the temperature to the 75−100 °C range leads to the de-esterification of the sulfonic acid groups, detaching them from the CW surface, and allowing them to catalyze the polymerization of FA.

The rapid progress of resinification is shown in Figure 4, which compares the FTIR spectra for FA with 0.75 phr CW after 1 h at 50 °C (spectrum a) and after reacting the CW-FA mixture at 100 °C for 30 min, 1 h, and 2 h (spectra b, c, and d,

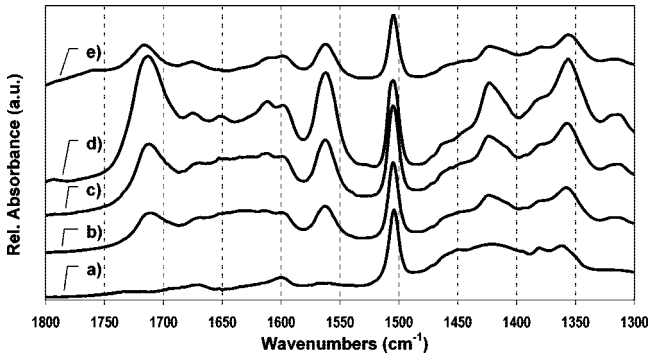

Figure 4. FTIR spectra for (a) CW-FA at 50 °C for 1 h; (b) CW PFA resin after reaction at 100 °C for 30 min; (c) CW PFA resin after reaction at 100 °C for 1 h; (d) CW PFA resin after reaction at 100 °C for 2 h; (e) for comparison, GAl PFA, that is, FA resinified with γ-Al at 100 °C for 12 h.

Table 1. Internal Referencing of the 1562 and 1712 cm^{-1} Peaks from Figure 5

peak height ratio I/I_{ref}	GAl-PFA 12 h/100 °C	CW-PFA 0.5 h/100 °C	CW-PFA 1 h/100 °C	CW-PFA 2 h/100 °C
I_{1562}/I_{1500}	0.527	0.465	0.663	1.107
I_{1712}/I_{1500}	0.424	0.455	0.697	1.349

respectively). The spectrum for pure PFA after 12 h resinification with γ-Al catalyst at 100 °C (spectrum e) is included for comparison and coded GAl-PFA. The polymerization of FA is typically accompanied by significant increases in the intensity of the peak at 1562 cm^{-1}, assigned to the skeletal vibration of 2,5 disubstituted furan rings, and at 1712 cm^{-1}, assigned to the C=O stretch of γ-diketones formed from hydrolytic ring opening of some of the furan rings along the PFA chain.[9,11] At the same time, there is a decrease in peak intensity (not shown) for the broad peak in the hydroxyl stretching region (3200−3600 cm^{-1}) and for the peak at 3120 cm^{-1}, assigned to the in-plane stretch of the hydrogen at the C5 position of the furan ring.[21] The intensity of the sharp peaks at 1504 cm^{-1}, assigned to ring stretching of the furan ring serves as an internal reference peak for semiquantitative analysis. Table 1 shows the results of applying the internal referencing method to the peaks at 1562 cm^{-1} and 1712 cm^{-1} for the spectra in Figure 4. Internal referencing of the 1562 cm^{-1} peak to the 1500 cm^{-1} peak indicates that in less than 1 h at 100 °C, the degree of polymerization of the CW-PFA resin is comparable to GAl-PFA resin after 12 h resinification at 100 °C. This is also apparent from internal referencing of the 1712 cm^{-1} peak to the 1500 cm^{-1} peak.

3.3. Increased Thermal Stability of Polyfurfuryl Alcohol Nanocomposites. Common applications of PFA include adhesives, corrosion resistant coatings and composites, as a binder material in foundry cores and in other applications where its inherent flame retardancy, low smoke release and high char yield are desired. On the other hand, MMT is often used to enhance the thermal properties of a composite material. Significant increases in the onset of decomposition and char retention have been described for a range of PNCs using MMT.[5,22] This is generally attributed to the ability of MMT to function as a mass transport barrier, hindering the out-diffusion of decomposition products, and to the restricted thermal motion of polymer chains at the MMT surface. To characterize the thermal resistance of cured PNCs, the MMT-PFA and CW-PFA resins were oven-cured in two stages, first at 130 °C for 75 min, and then at 210 °C for 105 min. GAl-PFA was cured under the same conditions, to provide a basis for comparison. In CW-PFA nanocomposites, the ability of CW to increase the thermal stability of a PNC by restricting the thermal motion of the matrix polymer is evident

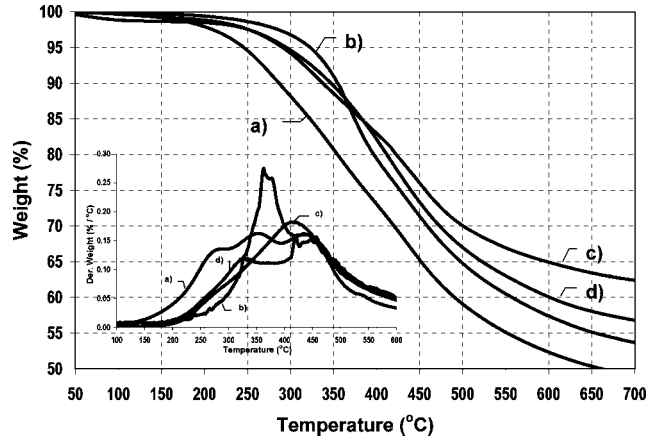

Figure 5. TGA scans collected at 10 °C/min showing onset of degradation for the case of nonoxidative degradation in N_2 for cured PNCs of (a) GAl-PFA, (b) CW-PFA, (c) 30BMMT-PFA, and (d) NaMMT PFA. The inset represents the derivative (d(weight %)/dT) of the degradation profiles.

Table 2. Temperature at Onset of Decomposition and Weight Retention at 500 and 800 °C for Cured PFA Nanocomposites

	Gal-PFA	CW-PFA	NaMMT-PFA	30BMMT-PFA
Onset of Degradation (5% Weight Loss) in N_2 Flow				
	246 °C	323 °C	302 °C	295 °C
Weight Retained after Nonoxidative Degradation in N_2				
500 °C[a]	59%	65%	67%	70%
800 °C[b]	48%	52%	55%	60%

[a] Standard deviation for residual weights is 1.0%. [b] Standard deviation for residual weights is 1.3%.

from the TGA spectra shown below in Figure 5. Figure 5 shows nonoxidative degradation of GAl-PFA (spectrum a), CW-PFA (spectrum b), 30BMMT-PFA (spectrum c), and NaMMT-PFA (spectrum d). In CW-PFA, the onset of degradation (temperature at 5% weight loss) is 323 °C, which is 77 °C higher compared to GAl-PFA, and also 20−30 °C higher compared to the MMT-PFA nanocomposites. Above 400 °C, however, 30BMMT-PFA shows the highest thermal stability of all three PNCs. Table 2 shows weight retention at 500 and 800 °C for cured PFA nanocomposites. At 800 °C, the residual mass of 30BMMT-PFA is 12% higher compared to GAl-PFA. The increased thermal resistance of the MMT-PFA nanocomposites compared to CW-PFA nanocomposites can be attributed to the retarded out-diffusion of decomposition products thanks to the "labyrinth" morphology of exfoliated MMT in the matrix.[14] Above 450 °C, H_2O evolved from the decomposing PFA, tends to oxidize methylene bridges between furan rings to carbonyl functions.[23,24] Hence, the longer diffusion path in MMT-PFA nanocomposites translates to a greater likelihood of oxidation of PFA with H_2O, as opposed to mass loss of H_2O. The explanation for the increased thermal resistance of 30BMMT-PFA nanocomposite as compared to the NaMMT-PFA nanocomposite is less straightforward. Tentatively, we propose that since exfoliation of NaMMT occurs while the PFA is still resinous, this allows for a small amount of phase separation of the NaMMT to occur prior to final matrix consolidation. NaMMT has a hydrophilic surface, and is less compatible with the organophilic PFA matrix compared to the 30BMMT. Phase separation of the NaMMT may result in gaps in the labyrinth morphology through which diffusion is more rapid. In contrast, organophilic 30BMMT exfoliates during the late cure stage, and the exfoliated morphology of the 30BMMT is locked in place by the low mobility of the highly branched and cross-linked PFA matrix.

4. Conclusions

In conclusion, we have produced two new types of biobased PNCs by using in situ polymerization techniques to disperse nanoparticles of CW or MMT in a thermosetting PFA matrix. In situ polymerization with CW or MMT offers an attractive processing route for producing PFA matrix nanocomposites without the use of solvents or surfactants. Both CW and MMT play a dual role in the in situ polymerization process, by first catalyzing the polymerization, thereby eliminating the use of strong mineral acid catalysts, and then enhancing the thermal stability of the consolidated PNCs. The highest increase in the temperature at onset of degradation is seen for CW-PNCs, which increase the onset temperature by nearly 80 °C, at only 0.75 wt %. However, the highest increase in residual weight above 400 °C is seen for the MMT-PFA nanocomposites. Future work will aim at the mechanical behavior of these PNCs, which tie together the objectives of increasing the use of usage of biobased materials while realizing advanced composite materials by using nanoscale fillers.

Acknowledgment. This research was supported in part by a research grant from the Institute of Paper Science and Technology (IPST) at the Georgia Institute of Technology, by a Graduate Scholarship from the Institute of Paper Science and Technology (IPST) at the Georgia Institute of Technology (to L.P.) and by the European Union Marie Curie International Reintegration Grant (IRG), Nr. 036577. The montmorillonite clay used in this work, Cloisite (R) Na+ and Cloisite (R) 30B, was a generous gift from Southern Clay Products, Inc.

Supporting Information Available: DSC traces of the effect of MMT catalyst on resinification of FA. This material is available free of charge via the Internet at http://pubs.acs.org.

References and Notes

(1) Chazeau, L.; Cavaille, J. Y.; Canova, G.; Dendievel, R.; Boutherin, B. *J. Appl. Polym. Sci.* **1999**, *71* (11), 1797.
(2) Dufresne, A.; Kellerhals, M. B.; Witholt, B. *Macromolecules* **1999**, *32* (22), 7396.
(3) Luo, J.-J.; Daniel, I. M. *Compos. Sci. Technol.* **2003**, *63* (11), 1607.
(4) Terech, P.; Chazeau, L.; Cavaille, J. Y. *Macromolecules* **1999**, *32* (6), 1872.
(5) Alexandre, M.; Dubois, P. *Mater. Sci. Eng., R* **2000**, *28* (1−2), 1.
(6) Dubief, D.; Samain, E.; Dufresne, A. *Macromolecules* **1999**, *32* (18), 5765.
(7) Mohanty, A. K.; Misra, M.; Drzal, L. T. *J. Polym. Environ.* **2002**, *10* (1−2)), 19.
(8) Dunlop, A. P.; Peters, F. N. *The Furans*; ACS Monograph 119; American Chemical Society, Reinhold Pub. Corp.: New York, 1953; Chapter 8.
(9) Conley, R. T.; Metil, I. *J. Appl. Polym. Sci.* **1963**, *7* (1), 37.
(10) Choura, M.; Belgacem, N. M.; Gandini, A. *Macromolecules* **1996**, *29* (11), 3839.
(11) Chuang, I. S.; Maciel, G. E.; Myers, G. E. *Macromolecules* **1984**, *17* (5), 1087.
(12) Principe, M.; Ortiz, P.; Martinez, R. *Polym. Int.* **1999**, *48* (8), 637.
(13) Podsiadlo, P.; Kaushik, A.; Arruda, E.; Waas, A.; Shim, B.; Xu, J.; Nandivada, H.; Pumplin, B.; Lahann, J.; Ramamoorthy, A.; Kotov, N. *Science* **2007**, *318* (5847), 80.
(14) LeBaron, P. C.; Wang, Z.; Pinnavaia, T. J. *Appl. Clay Sci.* **1999**, *15* (1−2), 11–29.
(15) Park, J. H.; Jana, S. C. *Macromolecules* **2003**, *36* (8), 2758.
(16) Wang, Z.; Pinnavaia, T. J. *Chem. Mater.* **1998**, *10* (12), 3769.
(17) Kvien, I.; Oksman, K. *Appl. Phys. A: Mater. Sci. Process.* **2007**, *87* (4), 641.
(18) Brechet, Y.; Cavaille, J. Y.; Chabert, E.; Chazeau, L.; Dendievel, R.; Flandin, L.; Gauthier, C. *Adv. Eng. Mater.* **2001**, *3* (8), 571.
(19) Noishiki, Y.; Nishiyama, Y.; Wada, M.; Kuga, S.; Magoshi, J. *J. Appl. Polym. Sci.* **2002**, *86* (13), 3425.
(20) Svagan, A. J.; Samir, M. A. S. A.; Berglund, L. A. *Adv. Mater.* **2008**, *20* (7), 1263.
(21) Yao, J.; Wang, H.; Liu, J.; Chan, K.; Zhang, L.; Xu, N. *Carbon* **2005**, *43* (8), 1709–1715.
(22) Ray, S. S.; Okamoto, M. *Prog. Polym. Sci.* **2003**, *28* (11), 1539.
(23) Fitzer, E.; Schaefer, W. *Carbon* **1970**, *8* (3), 353.
(24) Gaefke, C. B.; Botelho, E.; Ferreira, N.; Rezende, M. *J. Appl. Polym. Sci.* **2007**, *106* (4), 2274.

MA8020213